Progress on Multielement Spectroscopic Temperature and Impurity Studies on a High Flow Velocity Z-Pinch

Aidan W. Klemmer, *Graduate Student Member, IEEE*, Stephan Fuelling, Bruno S. Bauer, Glen A. Wurden, *Senior Member, IEEE*, Andrew S. Taylor, Derek A. Sutherland, Aaron Hossack, Uri Shumlak, *Fellow, IEEE*, Ben J. Levitt, Brian A. Nelson, Morgan Quinley, Tobin R. Weber, Jared Smythe, Bennett Diamond, Marcus Parry, and Clemente Parga

(Invited Paper)

***Abstract*— Multiple spectroscopy diagnostics have been fielded on the FuZE-Q sheared-flow-stabilized (SFS) Z-pinch to measure plasma impurities, flow velocity, temperature, and density. The spectroscopy diagnostics currently cover the wavelengths from extreme ultraviolet (EUV) in the 5–40 nm (30–250 eV) range, ion Doppler spectroscopy (IDS) in the 225–233 nm range, to compact broadband spectroscopy (UV/VIS) in the 220–1050 nm range. Spectral databases and collisional-radiative (CR) modeling have been used to identify impurities and estimate plasma parameters. Many emission lines from deuterium (D), carbon (C), and oxygen (O) have been identified, at this time. Current line-emission spectroscopy is sensitive to relatively low temperatures characteristic of the edge plasma, outside the fusion core. Temperature estimates using O as an EUV spectroscopic tracer have been compared to IDS estimates using C. EUV and IDS spectra find evidence of an ensemble of edge plasma temperatures in device-commissioning shots. Modeling line pairs involving B-like, Be-like, Li-like, and He-like O yielded electron temperatures from 16 to 155 eV. This profile is comparable to ion temperatures observed by IDS from Doppler broadening of Be-like C (34 eV) and He-like C (298 eV). Deposition and debris from within FuZE-Q have been analyzed with scanning electron microscope (SEM) energy dispersive X-ray spectroscopy (EDS) and find evidence of C, O, Si, W, Al, Cu, Fe, and Cr. Synthetic spectra from CR modeling, informed by plasma numerical simulations, can be compared to experimental spectra and thereby benchmark the calculations. Measurements of the edge plasma provide insight into plasma-wall interactions. Impurity identification is vital for radiative power and scientific Q calculations.**

***Index Terms*— Collisional-radiative (CR) modeling, fusion energy, FuZE-Q, plasma impurities, plasma spectroscopy, sheared-flow, Z-pinch.**

Manuscript received 28 August 2023; revised 24 November 2023; accepted 29 December 2023. Date of publication 30 January 2024; date of current version 21 June 2024. This work was supported in part by the U.S. Department of Energy through ARPA-E under Award DE-AR0001161 and Award DE-AR0001267; in part by the Los Alamos National Laboratory (LANL) under Grant BETHE DOE-FOA-2212-1526; and in part by Zap Energy, Inc. LANL is operated by Triad National Security, LLC, for the National Nuclear Security Administration of the U.S. Department of Energy under Contract 89233218CNA000001. The review of this article was arranged by Senior Editor S. J. Gitomer. *(Corresponding author: Aidan W. Klemmer.)*

Aidan W. Klemmer, Stephan Fuelling, and Bruno S. Bauer are with the Department of Physics, University of Nevada, Reno, NV 89557 USA (e-mail: aidan@nevada.unr.edu).

Glen A. Wurden is with the Los Alamos National Laboratory, Los Alamos, NM 87545 USA.

Andrew S. Taylor, Derek A. Sutherland, Aaron Hossack, Ben J. Levitt, Brian A. Nelson, Morgan Quinley, Tobin Weber, Marcus Parry, and Clemente Parga are with Zap Energy Inc., Seattle, WA 98104 USA.

Uri Shumlak, Jared Smythe, and Bennett Diamond are with the Aerospace and Energetics Research Program, University of Washington, Seattle, WA 98195 USA, and also with Zap Energy Inc., Seattle, WA 98104 USA.

Color versions of one or more figures in this article are available at https://doi.org/10.1109/TPS.2024.3354119.

Digital Object Identifier 10.1109/TPS.2024.3354119

I. Introduction

THE Z-pinch has been studied historically [1], [2] and has seen a resurgence of interest recently for its potential in low-cost fusion energy. While the static Z-pinch is inherently unstable, by introducing sheared-flow it is possible to dramatically reduce the $m = 0$ and $m = 1$ instabilities in a Z-pinch [3], [4], [5], [6]. Sheared-flow-stabilized (SFS) Z-pinch technology has progressed from university scale experiments to scientific break-even relevant devices [7]. During this time, much progress has been made in studying Zap Energy's Z-pinch devices, FuZE and FuZE-Q, and diagnosing their plasma parameters. On FuZE, plasma electron temperatures between 167 ± 16 eV and 700 ± 85 eV and densities of $\leq 5 \times 10^{16}$ cm^{-3} have been measured with optical Thomson scattering (OTS) [8]. More recently, electron temperatures in the range of 1–3 keV have been measured with OTS on higher performance FuZE plasmas [9]. Additional measurements include plasma ion temperatures of ~1–2 keV and densities of $\sim 10^{17}$ cm^{-3} [10]. Plasma flow velocities as high as 240 km/s have been measured with IDS [11], [12], [13] on FuZE. Thermonuclear neutron production is supported by data from neutron energy anisotropy studies [14].

As this technology scales to higher fusion triple-products ($nT\tau$), the importance of plasma parameter measurements scales similarly. The need for temperature measurements in a fusion plasma is evident, and thus an ongoing focus on FuZE-Q. Measurements of radial sheared-flow in the plasma are more unique to SFS devices but are also critical. Additionally, plasma impurity studies are important for future scientific gain calculations in SFS Z-pinch devices [15]. Here,

we present early spectroscopic temperature and impurity measurements from the FuZE-Q device, focusing on the boundary plasma that provides insight into plasma–wall interactions.

This article is organized in the following manner. The result of impurities on parameters affecting the scientific Q of a high flow velocity Z-pinch is introduced in Section II. Section III describes the EUV spectroscopy diagnostic and supporting collisional-radiative (CR) modeling. Electron temperatures from an eight-shot FuZE-Q commissioning campaign are calculated and presented. Section IV describes ion temperature measurements from the IDS diagnostic for the same shot series. Section V describes early impurity identification efforts on FuZE-Q. Deposition and debris found within the devices are analyzed with scanning electron microscopy and energy dispersive spectroscopy (EDS), corroborating spectroscopic impurity identification. The experimental results from multiple diagnostics on FuZE-Q are discussed in Section VI. Section VII summarizes the presented work.

II. Effect of Impurities on Scientific Q

It is important to understand the effect of plasma impurity levels on the average charge state, $\bar{Z}$, and effective ionization state, Z_{eff}, to understand the conditions needed to reach scientific equivalent $Q = 1$ [15] in an SFS Z-pinch. Many factors are influenced by $\bar{Z}$ including the Alfvén speed, v_A, that is related to the sound speed, c_s (in an SFS Z-pinch with $\beta \approx 1$ [16]), and is modified by $\bar{Z}$. The Alfvén speed is an important parameter for the stability requirement for an SFS Z-pinch.

Linear MHD stability analysis [4] suggests the Mach number required to stabilize the $m = 1$ mode in a sheared-flow Z-pinch. The Mach number, C_m, defines the minimum required axial flow velocity needed for sheared-flow stabilization, as a function of average state charge, $\bar{Z}$, axial wavenumber, k, pinch radius, a, and sound speed, c_s. Typically, $C_m = 0.1$ is assumed, however, $C_m > 0.1$ may be more accurate for some operational regimes on the FuZE and FuZE-Q devices [17]. Numerical studies with the Magneto-Hydro-Radiative-Dynamics Research (MHRDR) code [18] found that linear flow profiles are more efficient in stabilizing internal $m = 0$ modes than parabolic profiles [19], [20]. The stabilizing effects of sheared-flow studied in MHRDR [19], [20] are similar to those studied with MACH2 [21] in Shumlak et al. [22].

Following the methodology outlined by Shumlak et al. [15], the scientific equivalent Q for a D-T fusion SFS Z-pinch can be calculated for a set of plasma parameters. The plasma flow power (the steady-state rate of kinetic energy supplied), P_{flow}, and radiative power, P_{rad}, are two important terms in scientific equivalent Q calculations, and are defined in (15) and (19) of [15], respectively. The assumption that P_{rad} is well approximated by bremsstrahlung is accurate for highly ionized plasmas. However, in systems with less highly ionized plasmas, line radiation will grow increasingly important. The axial flow velocity, v_z, modifies P_{flow} and has an important effect on Q. In experiments, flow velocities as high as 240 km/s have been measured [11], but typical velocities on FuZE are closer to 100 km/s. The SFS Z-pinch flow velocity is measured primarily with IDS [13]. However, some

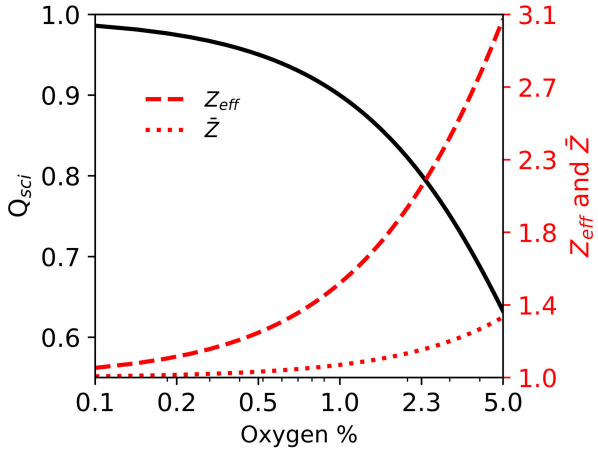

Fig. 1. Effect of varying oxygen impurity level on the SFS Z-pinch scientific Q (black) at 5 keV and 5×10^{19} cm^{-3}. The relationship between the oxygen impurity percentage and $\bar{Z}$, (red dotted), and Z_{eff} (red dashed), is shown. The calculations used a pinch radius of 0.5 cm, length of 0.5 m, and stability requirement $C_m = 0.1$. Scientific Q is highly sensitive to impurities and drops rapidly with increasing oxygen percentage.

analyses have used high-speed camera images to track plasma emission features and allow flow velocity measurements [11]. Given the complexity of these calculations, it is prudent to investigate the similarities and differences between line-of-sight, radially integrated IDS (usually using carbon impurity emission) flow velocity measurements and those made with other diagnostics such as high-speed cameras. More discussion of the diagnostics and impurities in the SFS Z-pinch follows in the next sections.

In addition to flow velocity, the average charge state, $\bar{Z}$, and the effective ionization state, Z_{eff}, also contribute to a number of calculations including scientific Q. Impurities in a plasma contribute additional electrons as they are ionized in the plasma. This effect can be dramatic as many fusion plasma impurities have high atomic numbers ("high-Z"). As a result, impurities increase the number of electrons beyond those from the fusion fuel such that $n_e > n$. An example of the effects of oxygen impurity levels on scientific Q, Q_{sci}, is shown in Fig. 1. $\bar{Z}$, and Z_{eff} are calculated as functions of the oxygen impurity fraction. For the SFS Z-pinch scientific $Q = 1$ regime at 5 keV and 5×10^{19} cm^{-3}, the $\bar{Z}$ and Z_{eff} are plotted together, along with Q_{sci}, in Fig. 1. A 0.5 cm plasma pinch radius, 0.5 m pinch length, L, and alpha heating fraction, $f_c = 0$, have been used for these calculations. Here, we assume fully ionized DT fuel (50%–50% D-T) and impurity populations for simplicity. The confinement time is approximated as the axial flow through time, $\tau = L/v_z$.

It is challenging to make accurate calculations of $\bar{Z}$ or Z_{eff}, usually requiring the use of one or more absolutely calibrated spectrometers. One option is Survey, Poor Resolution, Extended Domain (SPRED) spectroscopy techniques [24]. CR modeling [25], [26] may aid analysis, but requires knowledge of the underlying atomic physics of the plasma. If appropriate, charge exchange recombination spectroscopy techniques can also be used [27]. Some Z_{eff} calculations use multidisciplinary approaches that analyze data from multiple diagnostics and implement Integrated Data Analysis (IDA)

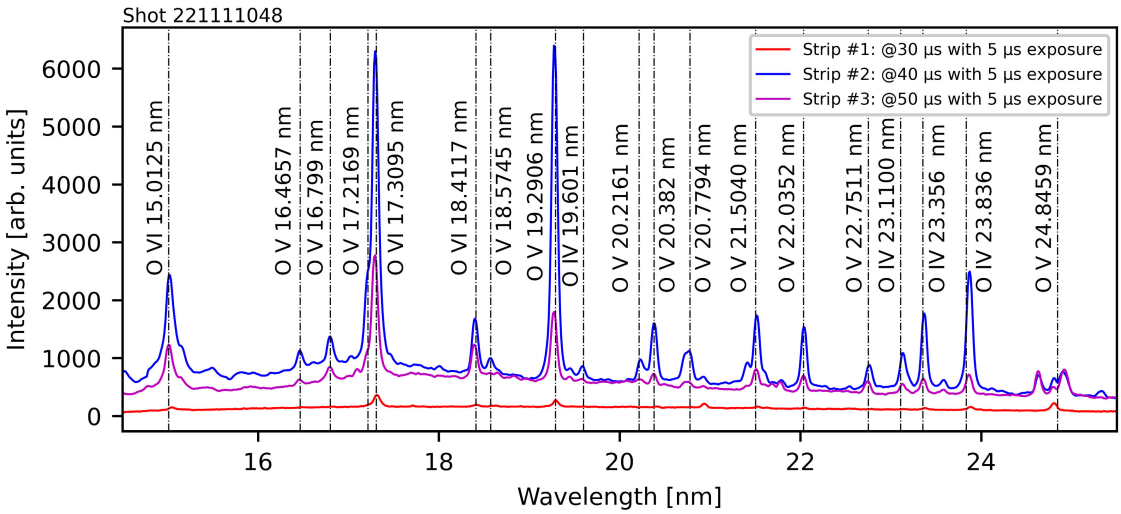

Fig. 2. Spectra from the EUV spectrometer diagnostic on FuZE-Q [23]. Suggested line emission identification for shot 221111048 finds a range of oxygen ions from B- to Li-like O (O IV–O VI) between ∼15 and 25 nm. Three spectra are shown, collected during the same shot, but at different times (30, 40, and 50 μs).

techniques in the framework of Bayesian Probability Theory (BPT) [28], [29]. In general, these approaches use more than one spectrometer, in different physical locations of the experiment and sensitive in the extreme ultraviolet (EUV) to infrared (IR) wavelength ranges, to estimate Z_{eff}.

III. EUV Spectroscopy Diagnostic

To aid advanced spectroscopic measurements on FuZE-Q a diagnostic for EUV spectroscopy was designed, built, and fielded [23]. The diffraction grating provides sensitivity to EUV/SXR radiation in the 5–40 nm (30–250 eV) range. The spectrometer also features a multistrip microchannel plate (MCP) allowing the plasma emission spectra to be time-gated independently. By staggering the timing of the HV pulses during a FuZE-Q shot, the diagnostic can gather three spectra per shot in the 5–40-nm wavelength range (in ∼10 nm sections), see Fig. 2. The EUV spectrometer has proven to be highly robust to the fast pressure surge, and high deposition and debris environment found in FuZE-Q with data collected from over 1000 shots to date.

A. Framework for Comparison of Spectral Data to CR Modeling

Oxygen was identified in early EUV emission datasets (during the commissioning of FuZE-Q) [23] and was used as a spectroscopic tracer for plasma temperature estimates. Early EUV datasets were a good fit to low-temperature oxygen line radiation (see Fig. 2). Line identification efforts were aided by synthetic spectra from CR modeling in PrismSPECT [25], [30] and by data from the NIST spectral database [31]. The 5–40 nm (30–250 eV) range contains a variety of oxygen line emission including B-like through H-like oxygen (O IV–O VIII). To create synthetic spectra with PrismSPECT it is important to supply the program with an energy level structure and corresponding atomic cross sections and rate coefficients. Prism's Atomic Model Builder was used to create the atomic model using Prism's ATBASE data. Flexible

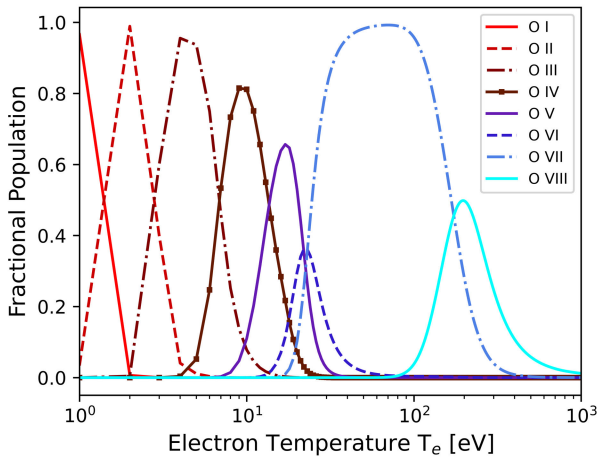

Fig. 3. Steady-state oxygen CSD at 10^{16} cm^{-3} as a function of electron temperature for each oxygen ion, calculated with PrismSPECT [30]. The horizontal axis (T_e) is shown with a logarithmic scale. A range of oxygen ions, B-like oxygen (O IV) through H-like oxygen (O VIII), provide temperature sensitivity below 1000 eV.

Atomic Code (FAC) data could be used for this analysis as well [32]. A comprehensive list of oxygen ions and transitions was included in the model.

The CR tool PrismSPECT was used to calculate synthetic spectra assuming a set of initial conditions. First, a "zero-width" optically thin geometry was chosen because radiative effects are not expected to contribute heavily to the overall EUV emission spectra (due to the low densities $<10^{17}$ cm^{-3}). Radiative effects may play an important role in modeling particularly dense short-lived regions of the plasma column, however, overall, the plasma was well modeled by the optically thin and highly collisional regimes. A steady-state nonlocal thermodynamic equilibrium (NLTE) calculation was used. The simulations assumed a 1% concentration of oxygen in a deuterium plasma with an ion density of 10^{16} cm^{-3}. Synthetic spectra were calculated with these conditions for different electron temperatures between 5 and 700 eV in steps of 1 eV. PrismSPECT produces charge state distributions (CSDs), Fig. 3, for a given ion and density as a function of temperature.

Several interesting observations can be made from the CSD. First, at relatively low temperatures of 5 eV, there are significant level populations in multiply ionized excited states. Second, from the perspective of a spectroscopic tracer, oxygen provides excellent temperature sensitivity between ∼1 and 100 eV as the dominant ion species evolves from O II to O VII. Finally, the relative populations of He- and H-like ions provide sensitivity to temperatures above ∼100 eV.

By collecting spectra at six different wavelength regions, from six different shots, a broadband composite spectrum can be created [23]. It is possible to analyze the composite spectra in their entirety, assuming the shot-to-shot variability is low, and the device parameters are similar. However, single temperature and density models are unlikely to be able to match the entire broadband composite with sufficient accuracy. Instead, multiple small sections from a single shot are analyzed and compared to similar calculations from another shot. This allows small "micro" sections of the spectrum to be analyzed individually and a distribution of temperatures and densities to be calculated.

There are relative strengths and weaknesses of both broadband and segmented fitting analysis. Broadband fitting with a single temperature and density may provide a reasonable estimate from the overall emission, but without sufficiently complex radially and temporally dependent inputs many smaller contributions to the spectrum may be missed. Additionally, some regions of the overall broadband spectrum may have little sensitivity to higher temperature contributions. For example, there are no H-like oxygen ground state transitions in the 5–40 nm range (ground state H-like O emits between ∼1.4 and 1.9 nm). There are other H-like O emission features (i.e., $n = 3 \rightarrow 2$ at ∼10.2 nm) in the 5–40 nm range, but these may not be sufficiently intense to be observed beyond the contributions from lower temperature line emissions or even the continuum. For more accurate plasma temperature estimates it is beneficial to include information gained both from the broadband and segmented fitting. For example, if comparing the relative intensities of different ion species, it is beneficial to look at as many different ions as possible, Fig. 4. For this work, a number of oxygen ions have been analyzed in detail from one wavelength region, see Fig. 2, which shows an example of spectra from this location.

The data and the synthetic spectra were compared quantitatively by scaling the intensity of the synthetic spectra with a scaling factor a. However, because the intensity of the emergent spectra calculated by PrismSPECT is in units of erg/(cm^2 × str × s × Å), and the exact parameters of the spectrometer diagnostic or emitting plasma are not well known, it is necessary to scale the intensity of the synthetic spectra by $a(T)$, Fig. 4(b). The best-fit scaling factor, a, as a function of temperature T, $a(T)$, was calculated with one parameter (degree of freedom) χ^2 minimization method. The standard deviation uncertainty is estimated from analysis of the continuum. The standard deviation is calculated from fitting a Gaussian to the histogram of the difference between a linear fit and the continuum emission. This estimate is assumed to be constant and not vary with photon energy, which is reasonable for these small analysis windows, <1 nm. For this analysis, the

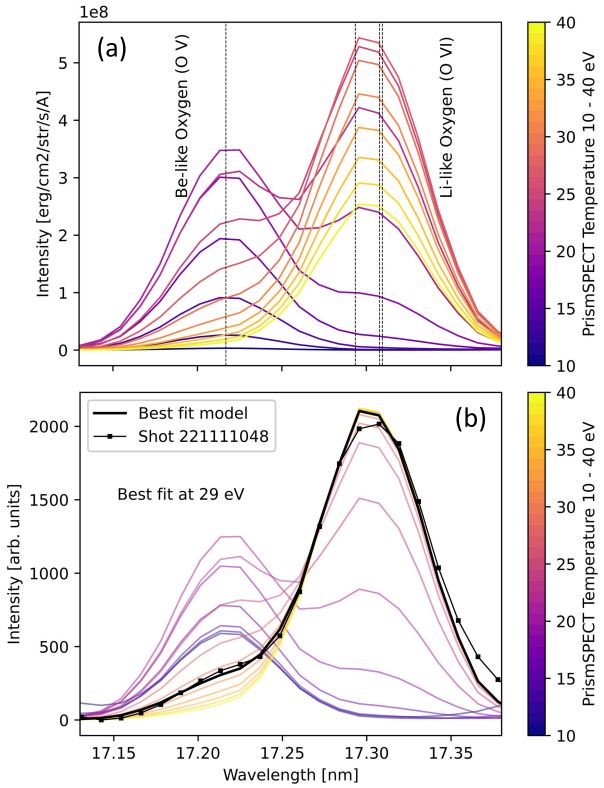

Fig. 4. Synthetic spectra from PrismSPECT [30] show the relative intensities of Be- and Li-like oxygen (a), as a function of electron temperature. The steady-state emergent spectra (a) are shown for temperatures between 10 and 40 eV. The calculations used 1% O and 99% D with a total ion density of 10^{16} cm^{-3}. The spectra have been adjusted to match the approximate resolving power of the EUV spectrometer (∼250). Experimental data from shot 221111048 strip #3 overlaid with the best fit model is shown in (b). The synthetic spectra in (b) have been scaled by the factor $a(T)$. The scaling factor $a(T)$, and the corresponding best fit temperature model, considering all temperatures (10–700 eV, in steps of 1 eV), was determined by χ^2 minimization. This method calculates the best fit at 29 eV of this shot.

degree of freedom (M) is 1. Furthermore, σ_i is a constant and not dependent on the index i, and is just σ. Thus, the analysis resembles a least-squares minimization. Since the continuum emission may have contributions from many temperatures and elements, the experimental data is normalized with an offset subtraction. The minimized χ^2 values calculated during this analysis were much larger than 1, and thus the best-fit models cannot be considered to be in strong agreement with the data. However, the fits are a general match to the data, and many of the χ^2 values calculated are reasonable. This work is intended to serve as a baseline framework for future EUV/X-ray measurements and analysis with improved methods and statistics.

Spectra collected with the EUV spectrometer are spatially integrated along a broad field of view, presenting difficulty for single-temperature spectroscopic data analysis. The single-temperature best-fit modeling here provides physically reasonable estimates but yields a distribution of temperatures. In addition, the relatively long exposures result in temporally integrated spectra. In regions of the spectrum with increased complexity, the effects of temporally and spatially integrated measurements are especially apparent. These effects can be reduced by shortening the exposure—the amount of time the spectra are integrated over.

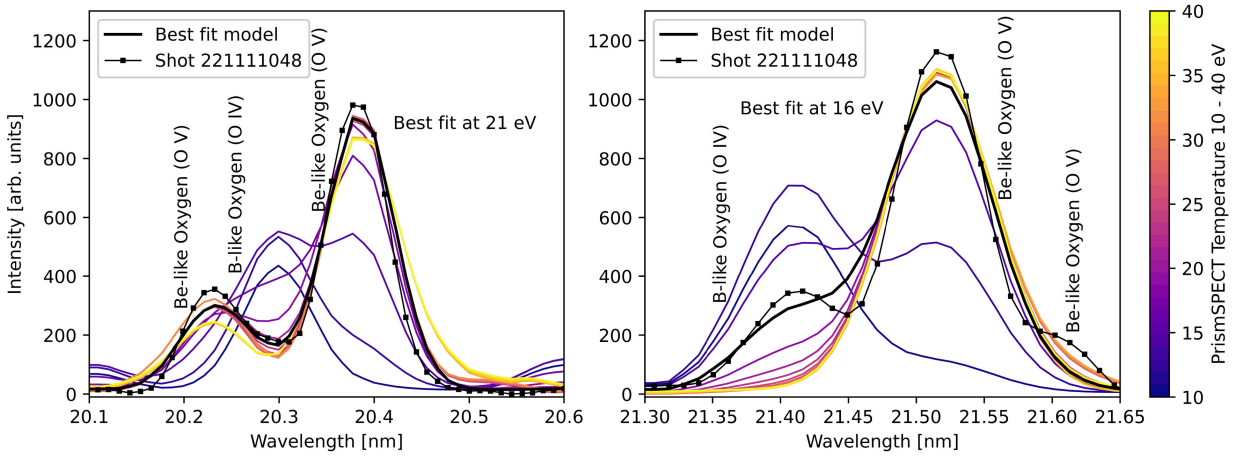

Fig. 5. Experimental data for shot 221111048 overlaid with the best fit synthetic spectra, for a range of temperatures. The best-fit model was determined by χ^2 minimization. Each tile shows a segment of the total spectrum collected for the shot. Several oxygen ions are easily identified including B-like O (O IV), Be-like O (O V), and Li-like O (O VI). The spectra are temporally integrated over 5 μs and spatially integrated over $\leq$ 20 cm.

B. Plasma Temperature Estimates via CR Modeling Comparison

By repeating this analysis over multiple locations within the emission spectrum, it is possible to study the ensemble of plasma temperatures within the field of view of the spectrometer. The emission spectra are spatially integrated along the field of view of the spectrometer, and temporally integrated due to relatively long exposures (of order microseconds), and thus it is likely that a given spectrum has contributions from an ensemble of temperatures and densities, not just one. These factors are important to consider when analyzing the EUV dataset.

The experimental setup of the EUV spectrometer on the FuZE-Q device at Zap Energy is discussed in detail in a previous publication [23], and therefore will only be briefly mentioned here. The EUV spectrometer was fielded at an angle 50° from the pinch axis, looking "downstream," to protect the spectrometer and reduce the amount of plasma entering the vacuum beamline. Due to this angle, the EUV spectrometer was sensitive to Doppler shifts from the moving radiating plasma inside the device. However, at this angle and at the flow velocities found within the FuZE-Q device this effect is expected to be small and is, of order, equal to the uncertainty in the calibration. However, this may contribute to the apparent redshifts seen when comparing the experimental data to the synthetic spectra from CR modeling. The plasma containing region of the FuZE-Q device is approximately 20 cm in diameter.

Examining the best-fit models calculated by reduced χ^2 minimization at four different regions within one spectrum (shot 221111048) it is possible to estimate a distribution of temperatures. For this FuZE-Q shot, the best-fit temperatures range from 16 to 29 eV, Figs. 4 and 5. The spectra from MCP strip #2 (Fig. 5) have been used for this analysis as its relative timing was set to correspond to the time of the main pinch event on FuZE-Q. This analysis suggests that it may be possible to study the ensemble of temperatures in the spatially and temporally integrated spectra by analysis of many individual components. Here, the ensemble of temperatures is

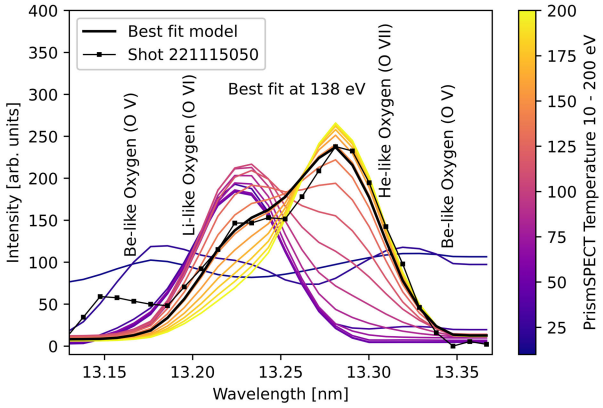

Fig. 6. Comparison of scaled synthetic spectra from PrismSPECT [30] to the experimental spectrum for shot 221115050. Contributions from Be-like, Li-like, and He-like O are observed in the experimental data. The color bar denotes the electron temperature of the synthetic spectra. The emergent spectra are shown for temperatures between 10 and 200 eV. The calculations used 1% O and 99% D with a total ion density of 10^{16} cm^{-3}. The spectra have been adjusted to match the expected resolving power of the EUV spectrometer ($\sim$250), and have been scaled by an arbitrary constant $a(T)$ to minimize the χ^2 value, between the synthetic and experimental data.

not only informed by contributions from one O ion but from many (in this case, O IV through O VI). O VI is the most heavily ionized oxygen ion observed in this shot. The lack of significant contributions from He- and H-like O for this shot, suggests that the edge plasma temperatures are <50 eV. For example, the numerous H-like O (O VIII) emission lines between $\sim$17.068 and $\sim$17.086 nm, and between $\sim$19.999 and $\sim$20.023 nm are absent in the data from this shot.

On another FuZE-Q shot (shot 221115050) emission spectra were collected in a different wavelength region than during shot 221111048. At shorter wavelengths, the EUV diagnostic is effectively more sensitive to higher energy radiation. The described analysis methods were repeated for the same spectral region at $\sim$17.3 nm, and also for a new region at $\sim$13.25 nm. The electron temperature estimated from CR modeling comparison at $\sim$17.3 nm is similar to shot 221111048, $\sim$25 eV. However, contributions from higher temperature regions of the plasma were also identified at $\sim$13.25 nm. The small region between 13.1 and 13.4 nm contains emission features

from multiple oxygen ions as a function of temperature. Contributions can be seen from Li-like (O VI) and He-like (O VII) oxygen, bounded by contributions from Be-like (O V) on either side, see Fig. 6.

Analysis of the spectral features around ∼13.25 nm finds temperatures of ∼138 eV, for this shot, see Fig. 6. Importantly, an ensemble of temperatures is evident in the experimental data, ranging from ∼25 eV based on analysis of O V and O VI at ∼17.3 nm, to ∼138 eV at ∼13.25 nm. Over the eight-shot series, the average best-fit electron temperature for the emission feature at ∼13.25 nm was 114 eV with a standard deviation of 17 eV. For the emission feature at ∼17.3 nm the average and standard deviation best-fit electron temperature was 28 ± 1 eV for the same shot series. It should be noted that these shots were part of early experimental campaigns during the device-commissioning of FuZE-Q in late 2022. The multiple plasma temperature estimates presented here are not expected to reflect the peak temperatures achieved in the core of the mega-ampere-scale Z-pinch.

The integrated temperature estimates from the EUV diagnostic can be bounded by other diagnostics such as OTS that provide highly localized temperature and density measurements. A suitable OTS system, similar to that fielded on FuZE [8], has been fielded on FuZE-Q and studies approximately the same axial position of the device as the EUV spectrometer. As this OTS diagnostic came online in early 2023, after the data presented herein was collected, comparative analysis between this EUV spectroscopy dataset and OTS is not possible. However, future work will include a comparison of radially integrated temperature measurements from the EUV spectrometer to the spatially resolved OTS temperature measurements on-axis. These experimental measurements, and others, can then be used to benchmark MHD simulations or other numerical modeling efforts [17], [33], [34], [35].

In more recent experimental campaigns, and with different gas puff and capacitor bank settings applied, the spectral signature of FuZE-Q has changed. As machine voltages and currents increased from late 2022 into 2023 a range of configurations and parameter spaces were investigated on FuZE-Q. The EUV spectrometer has collected data from thousands of shots over many of these configurations, parameter spaces, and experimental campaigns. The relative contribution of oxygen in the emission spectra appears to diminish in later EUV datasets. However, other impurities appear to be present in higher concentrations, as the overall complexity of the emission spectra has increased. Elements such as C, O, and Si do not appear to be solely responsible for the increased spectral complexity, but many emission lines have not yet been identified. The techniques used for the analysis of spectroscopic data rely on knowledge of the plasma constituents and thus future analysis will require intensive line-identification before current analysis methods can be used.

IV. Ion Doppler Spectroscopy

IDS has been a core diagnostic on many flow Z-pinch devices both at the University of Washington [5], [13], [36], [37], and at Zap Energy more recently [38]. It is the primary method for SFS Z-pinch flow velocity measurements. This diagnostic uses a set of telescopes, one Radial telescope oriented along the radial axis and one Oblique telescope oriented in the same axis but at an angle to the flow, typically 30° viewing upstream. Both are focused on the center of the chamber at the same location. Light collected in the Oblique telescope will be Doppler shifted from the motion of the emitting plasma and can be compared spectroscopically to the light from the Radial telescope, which has no wavelength shift. The telescopes image the spatially line integrated emission onto linear multifiber optical bundles. The design of these fiber bundle ferrules was improved dramatically in recent years. Bi- and quad-furcated fiber bundles allow light from both the Radial and Oblique telescopes to be analyzed simultaneously. To increase the radial spatial resolution, the current bundle includes 20 individual fibers per telescope. The fibers come together into a single ferrule with alternating Radial and Oblique cores in a linear pattern.

Light from the single ferrule is imaged onto the entrance slit of a high-resolution spectrograph (Princeton Instruments Isoplane 320 A, 3600 g/mm UV holographic diffraction grating, 20 μm entrance slit). The individual spectrum of each fiber is collected by a PI-MAX4 1024i P46 Intensified CCD camera for later analysis. The P46 phosphor provides the ability to collect two full-frame images only 1.5 μs apart. The IDS diagnostic is limited to measurements in the UV-VIS range of ∼200–900 nm by both the PI-MAX camera and fused silica vacuum windows on FuZE-Q, which significantly attenuate plasma emission at wavelengths shorter than ∼200 nm. The improved IDS system collects data with high spectral, temporal, and spatial resolution.

IDS results from one shot (221115050) are shown in Fig. 7. As with the presented EUV data, these data were collected in late 2022 during the device-commissioning of FuZE-Q. In Fig. 7, top, the raw image of all 40 fiber cores is presented along with the lineout of the Radial center chord (core 19) below. The C V ion emission at 227.091, 227.725, and 227.792 nm (around pixel 300) is used to infer plasma parameters, also shown in Fig. 7. The ion temperature from the Doppler broadening of the Radial chord line shape and ion velocity from the centroid shift of the Oblique chord line shape relative to its Radial partner are shown in Fig. 7. The center chord pair is aligned with $r = 0$ on axis. The rest of the chords provide measurements over $r = 0 \pm 7.6$ mm, for 15.2 mm total. The IDS spectra are typically collected at, or around, peak radiation time on FuZE-Q with exposure of 500 ns.

The ion flow velocity as a function of Oblique fiber position is also shown in Fig. 7, bottom. The Oblique chord fiber pairs are sensitive to Doppler shifts from the motion of the emitting plasma that, through comparison with the Radial chord, permits spatially resolved plasma velocity estimates. In this particular shot, the radial flow profile is asymmetric in the region $r = 0 \pm 7.6$ mm, likely due to fluctuations in the radial position of the plasma pinch. Other sheared-flow profiles can be found in literature [5]. For further discussion of flow velocities in sheared-flow Z-pinch experiments, see [11].

Plasma temperature estimates using C V, Fig. 7, find plasma ion temperatures between ∼150 and 200 eV, for this specific shot and 298 ± 26 eV (averaged over fiber chords and shots),

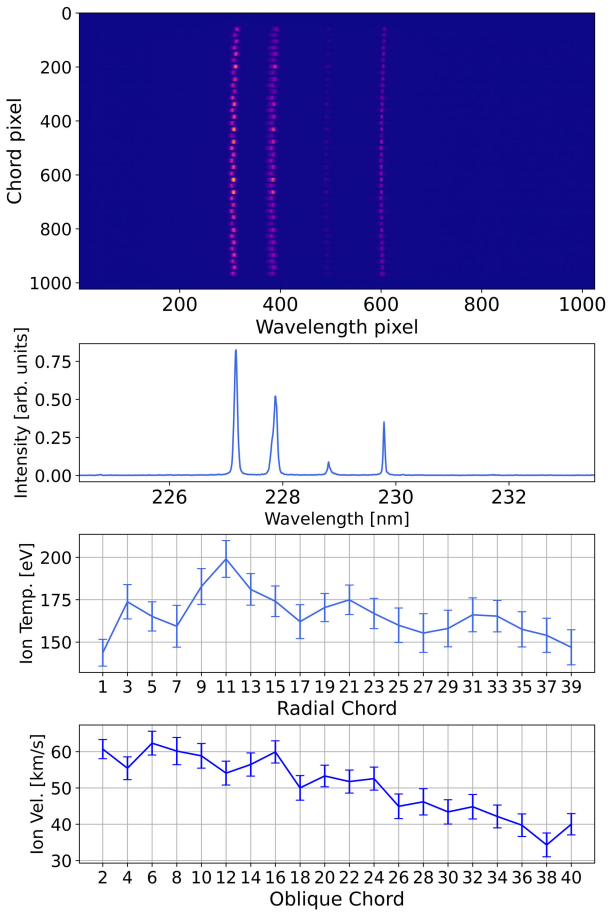

Fig. 7. IDS data from FuZE-Q. The raw image is shown (top), which spans the spectral range between approximately 225 and 231 nm. A lineout of the Radial center chord (core 19) from the image is shown in blue (middle top). Core 19 corresponds to approximately the radial center ($r = 0$) of FuZE-Q at the axial position P10 (10 cm downstream of the inner electrode "nosecone"). The measurements cover a radial distance of $\sim$ 15.2 mm and $r = 0 \pm 7.6$ mm. The ion temperature (from Doppler broadening) and velocity are calculated by fitting the C V (227.091, 227.725, and 227.792 nm) line shapes with Gaussian profiles. The difference in Doppler shifts between the Radial and Oblique chord pairs permits spatially resolved plasma flow velocity calculations. This data was collected in late 2022 during the device-commissioning of FuZE-Q.

for the eight-shot series. C III provides an attractive ion species for low-temperature spectroscopic studies in the UV range. Emission from C III at ~229 nm was also analyzed and is more sensitive to lower plasma temperatures. Analysis of the C III emission finds lower ion temperatures, 34 ± 7 eV, average and standard deviation, for the same eight-shot series.

V. Impurity Studies With Spectroscopic and Nonspectroscopic Methods

In addition to the EUV and IDS spectroscopy diagnostics, a compact broadband spectrometer sensitive in the UV/VIS wavelength range (220–1050 nm) has also been fielded on the FuZE and FuZE-Q devices. The spectrometer, an Ocean Insights HR2, is capable of exposures as short as 1 μs. The spectrometer has a spectral resolution of <1 nm FWHM and a 10 μm slit. The broadband spectra are taken in the assembly region of FuZE-Q with 1 μs exposures during key moments during a shot.

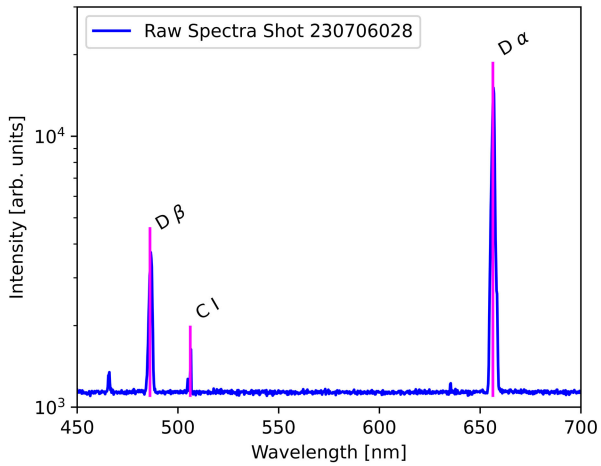

Fig. 8. Results for the high-resolution broadband UV/VIS spectroscopy diagnostic on FuZE-Q. An automated peak finding and identification algorithm has been developed to process spectroscopy data and is being tested on the broadband dataset.

An automated peak finding and identification algorithm has been developed to process the data from the broadband spectrometer, see Fig. 8. Spectral peaks with a sufficient prominence (above the noise threshold) are smoothed by a Savitzky–Golay filter and fit with a peak finding algorithm. Independently, the NIST atomic spectra database is queried, and the spectral lines associated with each element of interest (C, O, Si, Cu, etc.) are returned.

With the list of candidate peaks and candidate lines from NIST, the script then checks each candidate line to see if the line has an observed wavelength within the spectrometer's wavelength resolution (about 0.25 nm/pixel) and if the line has a suitable relative intensity. The remaining lines are then grouped into singlets, doublets, triplets, etc., based on matching the upper energy level and line species. The goodness of fit (GOF) is determined from converging fits by examining the normalized standard deviation of the width of the fit determined by the covariance matrix returned from the fitting algorithm.[1]

In the case of the plot shown in Fig. 8, the script has successfully identified all the lines associated with D α and D β as well as a C I singlet. Notably, the script misses a line from the C III triplet at ~485 nm. These lines are missing

[1]A synthetic spectrum of each set of candidate lines is created using a set of Gaussian functions. Each synthetic spectra set is simultaneously fitted to the raw spectrum, for all sets in the dataset. The wavelengths and relative amplitudes (based on the normalized relative intensity of each line as taken from NIST) of each line in the set are fixed, leaving only the widths and scaled amplitude of all the lines as free parameters for the fit. Peaks at or near the spectrometer's maximum counts are removed. The goodness of fit (GOF) is determined from converging fits by examining the normalized standard deviation of the width of the fit determined by the covariance matrix returned from the fitting algorithm (the scientific Python (scipy) "curve fit" function). This GOF metric will be minimized for lines that are well-defined and prominent. Lines that are not prominent enough above the continuum will not converge, or will have poor GOF. Spectral lines too close to the fitted line will broaden the Gaussian fit, making positive identification of the line less clear. Any line sets where the fit does not meet the empirically chosen GOF cutoff value are discarded. The remaining lines are then returned to the user as a table of lines and graphically as lines overlaid over the raw spectra from the spectrometer with each line labeled with the species and GOF metric. The script also includes a method that can return the number of lines found for a specifically requested species.

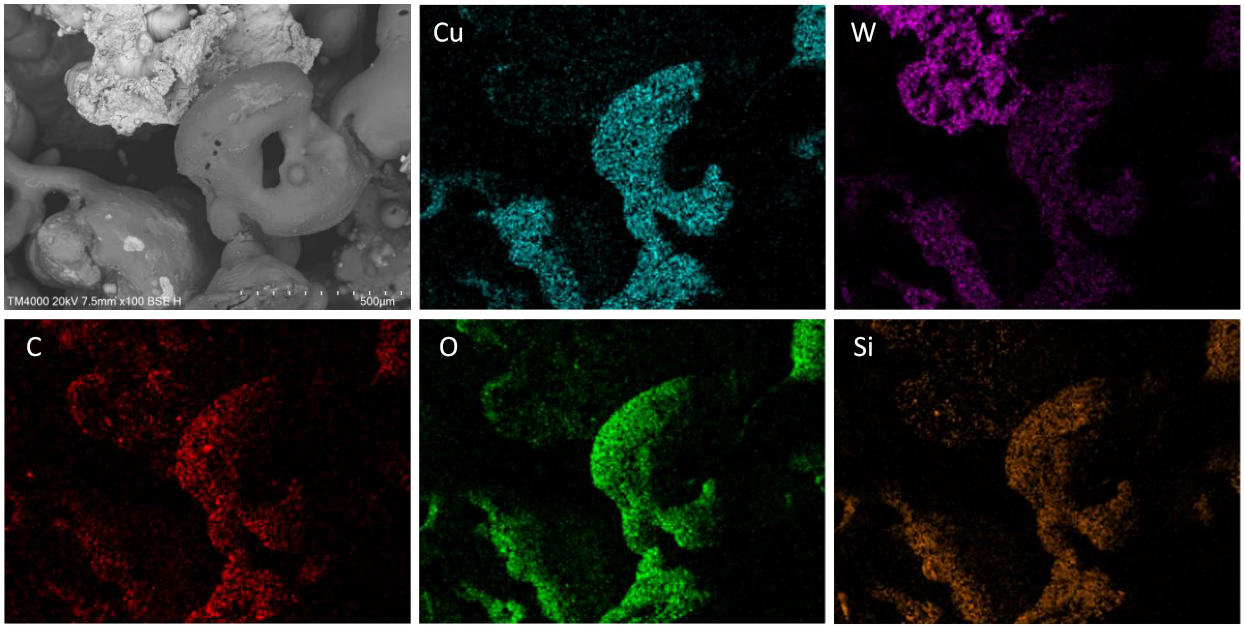

Fig. 9. Representative BSE SEM micrograph of collected FuZE-Q debris, alongside associated EDS compositional maps for the primary elements identified (Cu, W, C, O, and Si). Other elements identified in minor quantities include Al, Fe, and Cr.

because only one of the lines of the triplet was visible. The script attempted to fit the triplet, but because two of the lines in the triplet were not visible, the fit did not converge, and the script therefore removed that candidate line set.

This automated line identification technique, or improved versions of it, could be used to aid future analysis of the EUV and IDS spectrometer datasets. Additionally, the broadband UV/VIS spectrometer described is simple to field, extremely compact, and relatively inexpensive, making it an attractive option for future plasma measurements. Future work includes a comparison of plasma temperature and density estimates from the broadband UV/VIS spectrometer to the other EUV and IDS systems. Similarities or differences in the calculated results may allow for a more careful study of the plasma temperature and density distribution.

At Zap Energy Inc., a tabletop scanning electron microscope (SEM) was used to study the deposition and debris found within the FuZE and FuZE-Q devices, see Fig. 9. The Hitachi TM4000Plus SEM [39] is equipped with secondary electron (SE), backscattered electron (BSE), and mixed SE/BSE imaging capabilities. The SEM is also equipped with an energy dispersive X-ray spectroscopy (EDS) capability allowing the elemental composition of the sample to be studied in detail. The SEM uses an Oxford Instruments AZtecOne EDS [40]. After a significant number of shots, it is possible to identify deposition on the vacuum chamber windows of FuZE/FuZE-Q. Eventually, this degrades transmission enough to affect diagnostic performance (OTS, IDS, broadband UV/VIS spectroscopy, high-speed imaging, etc.) and requires window replacement or cleaning. In addition, eventually the bottom window on these devices collects debris that can be large, ~1 mm in scale. Some of this debris can be easily removed from the experimental devices and analyzed with SEM EDS.

The elemental composition of the debris from FuZE and FuZE-Q was analyzed with EDS and many elements were identified. In analysis of FuZE-Q debris over many experimental campaigns and many hundreds of shots, the primary elements identified are C, O, Si, W, and Cu, see Fig. 9. A range of elements were identified in smaller amounts including Al, Fe, and Cr. The complete EDS spectrum includes several elements not associated with fusion fuels. The presence of O and Si, along with other trace elements such as Na and K, can be explained by plasma–material interactions at the interface between the plasma and the vacuum chamber windows. Fused silica (quartz-SiO_2) is used in many vacuum chamber windows, along with borosilicate glass (silica, boric oxide, sodium oxide, potassium oxide, and aluminum oxide). Both fused silica (quartz) and borosilicate windows have been used on FuZE and FuZE-Q, historically. W, Al, Cu, Fe, and Cr are likely present from degradation of the vacuum and electrode/insulator materials in the devices.

Impurities in the FuZE and FuZE-Q devices are being studied with spectroscopic and nonspectroscopic techniques. As is common in many fusion experiments, plasma-material interactions introduce impurities into the fusion fuel that can be studied, if only indirectly, by analysis of deposition and debris found within the device. Nonspectroscopic studies corroborate spectroscopic measurements providing a more comprehensive picture of the impurities present within the fusion generator.

VI. Discussion of Results

Results are presented from several different spectroscopy diagnostics fielded on FuZE-Q. The utility of these instruments is demonstrated by their ability to study plasma velocity, temperature, and density. While the spectrometers study the plasma ion temperature directly, the electron temperature can be inferred by careful comparison to CR modeling results from PrismSPECT. The spectrometers are also capable of studying the elemental composition of the plasma for fusion plasma impurity studies. The SEM EDS analysis of deposition and debris found within the devices corroborates these spectroscopic impurities studies by confirming the presence of many

elements common in fusion generators via nonspectroscopic methods.

Analysis of the EUV spectrometer data finds emission contributions from a variety of oxygen ions corresponding to an ensemble of plasma temperatures. By collecting spectra at different regions of the EUV spectra between ∼5 and 40 nm it is possible to study a wide range of plasma emission energies. Emission lines associated with He-like O (O VII) are observed in some datasets, but there is no ground state He- and H-like O line emission in the ∼5–40 nm region. Future work will attempt to study the emission features at shorter wavelengths where greater sensitivity to higher plasma temperatures is expected. Depending on the radial temperature and density profile of the plasma within the EUV diagnostic's field of view these He- and H-like O emissions may be relatively small compared to the total emission continuum. For this admittedly limited study, the plasma density was held constant (10^{16} cm^{-3}) but may be a significant source of error in the calculations as the Z-pinch core is expected to be significantly more dense than the boundary plasma. Additionally, the simulations assumed a steady-state model without any time-dependent dynamics. Thus, the temperature estimates via CR modeling comparison presented here are likely underestimates. Future work will include CR modeling informed by MHD simulations that will more accurately model the radial temperature and density profiles and their time dependence.

Carbon is the primary element identified by IDS in the UV range (between ∼224 and 232 nm), whereas oxygen is the primary element identified by the EUV spectroscopy diagnostic (between ∼5 and 40 nm). These diagnostics look at approximately the same axial location of FuZE-Q, with spectra collected at approximately the same time. Given that IDS uses telescopes to collect light from a specific radial location on axis, $r = 0 \pm 7.6$ mm, it is much less sensitive to emission from the edge of the device. Tests found that the measured intensity dropped by approximately a factor of 2× for every 4″ away from the primary focal length of the IDS optics. This is important to remember when comparing the results from the EUV and IDS diagnostics. Carbon in these devices is largely sourced from the cathode nosecone and is expected to be drawn into the plasma pinch. In contrast, oxygen is likely sourced from plasma-material interactions at the windows and from degradation of an alumina insulator by the upstream electrodes and thus is not expected to be as heavily entrained in the plasma pinch as carbon. Some contributions from carbon are likely observed, but further line identification efforts are needed. In essence, the EUV diagnostic is line integrated along the entire field of view, whereas IDS is most sensitive to plasma emission on axis, and this difference may contribute to the differences in dominant emission seen, oxygen versus carbon.

Analysis of deposition and debris found within the FuZE and FuZE-Q devices provides an avenue for the study of the results from plasma-material interactions, and electrode and insulator degradation. The elements found within the deposition and debris in the devices may be compared and contrasted to the elements identified with spectroscopic measurements. From both a scientific and engineering standpoint, it is desirable to have multiple methods for studying the interactions of plasma and materials within a fusion generator.

The automated line identification currently in development and testing on the Ocean Insights UV/VIS spectrometer diagnostic will be important for future spectroscopic analysis. Future work aims to apply the identification techniques developed here to other spectroscopy diagnostics, such as the EUV and IDS systems. Additionally, it is interesting to calculate a variety of plasma parameters such as temperature and density from multiple spectroscopic diagnostics (EUV, IDS, Ocean Insights). Finally, impurity studies are crucial for calculating Z_{eff}, an important value for scientific Q in a fusion generator.

VII. Conclusion

Multiple spectrometers have been fielded on a high flow velocity Z-pinch to study plasma parameters such as temperature, density, and flow velocity. Spectroscopy is also an important tool for identifying impurities, which are critical to radiative power and scientific Q calculations in a fusion generator. Spectral databases and CR modeling have been used to help identify impurities and estimate plasma parameters. At this time, deuterium, carbon (C), and oxygen (O) have been definitively identified in the plasma line emission. Temperature estimates using O as an EUV spectroscopic tracer have been compared to IDS estimates using C. Current line-emission spectroscopy is sensitive to relatively low plasma temperatures at the edge of the device, outside the fusion core. Modeling line emission features in the EUV spectrometer data involving B-like, Be-like, Li-like, and He-like O yielded electron temperatures from 16 to 155 eV. This multitemperature profile is comparable to ion temperatures observed by IDS from Doppler broadening of Be-like C (34 eV) and He-like C (298 eV). SEM EDS analysis corroborates spectroscopic line identification, finding evidence of C, O, Si, W, Al, Cu, Fe, and Cr in the deposition and debris within FuZE-Q. Synthetic spectra from CR modeling, informed by plasma numerical calculations, can be compared to experimental spectra and thereby benchmark the calculations. Studies of low temperature edge plasma provide valuable insight into plasma-material interactions at the boundaries of the experimental device.

Acknowledgment

The authors would like to acknowledge and thank W. Cline, C. Davidson, A. Astanovitskiy, O. Dmitriev, K. Swanson, and R. Mancini from the University of Nevada, Reno. They also thank J. Coyne, W. McGehee, D. Austin, A. Johansen, A. D. Stepanov, K. Morgan, T. Gold, N. Pillai, L. Morton, A. P. Shah, D. Crews, C. Adams, E. Meier, P. Stoltz, K. Smith, and L. Pennings of Zap Energy, Inc.

References

[1] I. V. Kurchatov, "On the possibility of producing thermonuclear reactions in a gas discharge," *J. Nucl. Energy*, vol. 4, no. 2, pp. 193–202, Feb. 1957.

[2] W. H. Bennett, "Magnetically self-focussing streams," *Phys. Rev.*, vol. 45, no. 12, pp. 890–897, Jun. 1934.

[3] B. Kadomtsev, "Hydromagnetic stability of a plasma," *Rev. Plasma Phys.*, vol. 2, p. 153, 1966.

[4] U. Shumlak and C. W. Hartman, "Sheared flow stabilization of the $m = 1$ kink mode in Z pinches," *Phys. Rev. Lett.*, vol. 75, pp. 3285–3288, Oct. 1995.
[5] U. Shumlak, R. P. Golingo, B. A. Nelson, and D. J. Den Hartog, "Evidence of stabilization in the Z-pinch," *Phys. Rev. Lett.*, vol. 87, Oct. 2001, Art. no. 205005.
[6] T. D. Arber and D. F. Howell, "The effect of sheared axial flow on the linear stability of the Z-pinch," *Phys. Plasmas*, vol. 3, no. 2, pp. 554–560, Feb. 1996.
[7] U. Shumlak, "Z-pinch fusion," *J. Appl. Phys.*, vol. 127, May 2020, Art. no. 200901.
[8] J. T. Banasek et al., "Probing local electron temperature and density inside a sheared flow stabilized Z-pinch using portable optical Thomson scattering," *Rev. Sci. Instrum.*, vol. 94, no. 2, Feb. 2023, Art. no. 023508.
[9] B. Levitt et al., "Elevated electron temperature coincident with observed fusion reactions in a sheared-flow-stabilized Z pinch," Tech. Rep.
[10] Y. Zhang et al., "Sustained neutron production from a sheared-flow stabilized Z pinch," *Phys. Rev. Lett.*, vol. 122, no. 13, Apr. 2019, Art. no. 135001.
[11] A. D. Stepanov et al., "Flow Z-pinch plasma production on the FuZE experiment," *Phys. Plasmas*, vol. 27, no. 11, Nov. 2020, Art. no. 112503.
[12] E. L. Claveau et al., "Plasma exhaust in a sheared-flow-stabilized Z pinch," *Phys. Plasmas*, vol. 27, no. 9, Sep. 2020, Art. no. 092510.
[13] E. G. Forbes and U. Shumlak, "Spatio-temporal ion temperature and velocity measurements in a Z pinch using fast-framing spectroscopy," *Rev. Sci. Instrum.*, vol. 91, no. 8, Aug. 2020, Art. no. 083104.
[14] J. M. Mitrani et al., "Thermonuclear neutron emission from a sheared-flow stabilized Z-pinch," *Phys. Plasmas*, vol. 28, no. 11, Nov. 2021, Art. no. 112509.
[15] U. Shumlak, E. T. Meier, and B. J. Levitt, "Fusion gain and triple product for the sheared-flow-stabilized Z pinch," *Fusion Sci. Technol.*, vol. 80, no. 1, pp. 1–16, Jan. 2024.
[16] U. Shumlak et al., "Increasing plasma parameters using sheared flow stabilization of a Z-pinch," *Phys. Plasmas*, vol. 24, no. 5, Feb. 2017, Art. no. 055702.
[17] E. T. Meier and U. Shumlak, "Development of five-moment two-fluid modeling for Z-pinch physics," *Phys. Plasmas*, vol. 28, no. 9, Sep. 2021, Art. no. 092512.
[18] I. R. Lindemuth, *See National Technical Information Service*, document UCRL-52492, Lawrence Livermore Nat. Lab. UCRL-52492, Nat. Tech. Inf. Service, Springfield, Virginia, VA, USA, 1979.
[19] I. Paraschiv, B. S. Bauer, I. R. Lindemuth, and V. Makhin, "Linear and nonlinear development of m=0 instability in a diffuse Bennett Z-pinch equilibrium with sheared axial flow," *Phys. Plasmas*, vol. 17, no. 7, Jul. 2010, Art. no. 072107.
[20] I. Paraschiv, B. S. Bauer, I. R. Lindemuth, and V. Makhin, "Linear and nonlinear development of the $m = 0$ instability in Z-pinch equilibria with axial sheared flows," *J. Fusion Energy*, vol. 28, pp. 195–199, Jun. 2009.
[21] R. E. Peterkin, M. H. Frese, and C. R. Sovinec, "Transport of magnetic flux in an arbitrary coordinate ALE code," *J. Comput. Phys.*, vol. 140, no. 1, pp. 148–171, Feb. 1998.
[22] U. Shumlak et al., "Equilibrium, flow shear and stability measurements in the Z-pinch," *Nucl. Fusion*, vol. 49, no. 7, Jul. 2009, Art. no. 075039.
[23] A. W. Klemmer et al., "Implementation of extreme ultraviolet spectroscopy on a sheared-flow-stabilized Z pinch," *Rev. Sci. Instrum.*, vol. 94, no. 8, Aug. 2023, Art. no. 083507.
[24] D. G. Whyte, D. A. Humphreys, and P. L. Taylor, "Measurement of plasma electron temperature and effective charge during tokamak disruptions," *Phys. Plasmas*, vol. 7, no. 10, pp. 4052–4056, Oct. 2000.
[25] J. J. MacFarlane, I. E. Golovkin, P. R. Woodruff, S. K. Kulkarni, and I. M. Hall, "Simulation of plasma ionization and spectral properties with PrismSPECT," in *Proc. Abstr. IEEE Int. Conf. Plasma Sci. (ICOPS)*, 2013, doi: 10.1109/PLASMA.2013.6634781.
[26] H.-K. Chung, M. H. Chen, W. L. Morgan, Y. Ralchenko, and R. W. Lee, "FLYCHK: Generalized population kinetics and spectral model for rapid spectroscopic analysis for all elements," *High Energy Density Phys.*, vol. 1, no. 1, pp. 3–12, Dec. 2005.
[27] D. G. Whyte et al., "Measurement and verification ofzeffradial profiles using charge exchange recombination spectroscopy on DIII-D," *Nucl. Fusion*, vol. 38, no. 3, pp. 387–398, Mar. 1998.
[28] S. K. Rathgeber et al., "Estimation of profiles of the effective ion charge at ASDEX upgrade with integrated data analysis," *Plasma Phys. Controlled Fusion*, vol. 52, no. 9, Sep. 2010, Art. no. 095008.
[29] M. Krychowiak, R. König, T. Klinger, and R. Fischer, "Bayesian analysis of the effective charge from spectroscopic bremsstrahlung measurement in fusion plasmas," *J. Appl. Phys.*, vol. 96, no. 9, pp. 4784–4792, Nov. 2004.
[30] J. MacFarlane et al., "Simulation of the ionization dynamics of aluminum irradiated by intense short-pulse lasers," in *Proc. Inertial Fusion Sci. Appl.*, vol. 457, 2003.
[31] A. Kramida, Y. Ralchenko, and J. Reader. (May 8, 2023). *NIST Atomic Spectra Database (Ver. 5.10)*. National Institute of Standards and Technology, Gaithersburg, MD, USA. [Online]. Available: https://physics.nist.gov/asd
[32] M. F. Gu, "The flexible atomic code," *Can. J. Phys.*, vol. 86, no. 5, pp. 675–689, May 2008.
[33] I. A. M. Datta and U. Shumlak, "Computationally efficient high-fidelity plasma simulations by coupling multi-species kinetic and multi-fluid models on decomposed domains," *J. Comput. Phys.*, vol. 483, Jun. 2023, Art. no. 112073.
[34] K. Tummel et al., "Kinetic simulations of sheared flow stabilization in high-temperature Z-pinch plasmas," *Phys. Plasmas*, vol. 26, no. 6, Jun. 2019, Art. no. 062506.
[35] C. R. Sovinec et al., "Nonlinear magnetohydrodynamics simulation using high-order finite elements," *J. Comput. Phys.*, vol. 195, no. 1, pp. 355–386, 2004.
[36] D. J. D. Hartog and R. P. Golingo, "Telecentric viewing system for light collection from a z-pinch plasma," *Rev. Sci. Instrum.*, vol. 72, no. 4, pp. 2224–2225, Apr. 2001.
[37] R. P. Golingo and U. Shumlak, "Spatial deconvolution technique to obtain velocity profiles from chord integrated spectra," *Rev. Sci. Instrum.*, vol. 74, pp. 2332–2337, Apr. 2003.
[38] A. Taylor and A. W. Klemmer, "Optical tracking of low-Z impurities in a stabilized Z pinch through EUV-VIS emission," *Bull. Amer. Phys. Soc.*, 2022.
[39] *Hitachi TM4000II tabletop SEM*. Accessed: Jul. 2023. [Online]. Available: https://www.hitachi-hightech.com/global/en/products/microscopes/sem-tem-stem/tabletop-microscopes/tm4000ii.html
[40] *Oxford Instruments AZtecOne EDS*. Accessed: Jul. 2023. [Online]. Available: https://nano.oxinst.com/products/aztec/aztecone

Aidan W. Klemmer (Graduate Student Member, IEEE) received the B.A. degree in physics and astronomy (with a minor in mathematics) from the Earlham College, Richmond, IN, USA, in 2018. He is currently pursuing the Ph.D. degree with the University of Nevada, Reno, NV, USA.

During his doctoral studies he has held collaborations with scientists from Sandia, Los Alamos, NM, USA, and the Lawrence Livermore National Laboratory, Livermore, CA, USA, and has been involved in experiments on mega-ampere class Z-pinches, such as Mykonos, Zebra, and the Z-machine. His research has been concerned with plasma and high energy density physics of interest for fusion energy.

Stephan Fuelling was born in Solingen, Germany, in March 1955. He received the Diplom Physiker degree in experimental high-energy physics from the Rheinisch-Westfälische Technische Hochschule (RWTH) Aachen, Aachen, Germany, in 1984, and the Ph.D. degree in experimental atomic physics from the University of Nevada, Reno, NV, USA, in May 1991.

He worked as an Adjunct Professor with the Physics Department, University of Nevada, from 1991 to 2000. In 1994, he worked at McPherson, Inc., Acton, MA, USA. From 1996 to 2001, he worked on several research projects at the Electrical Engineering and the Physics Department, University of Nevada. From 2002 to 2015, he worked as a Research Assistant Professor with the Nevada Terawatt Facility, University of Nevada. His work involved plasma physics research and the development of plasma diagnostics, spectroscopy, mechanical and electronic designs, load hardware designs, for experiments on the Zebra 1 MA Z-pinch. Since 2020, he has worked in diagnostic development for Zap Energy, Inc., Everett, WA, USA, where he contributed to fielding an EUV spectrometer on their experimental fusion device FuZE-Q. In 2022, he worked as a consultant for Zap Energy, Inc., to develop other plasma diagnostics for FuZE-Q.

Bruno S. Bauer received the Ph.D. degree in plasma physics from the University of California, Los Angeles, CA, USA, in 1992.

He is currently a Professor of physics with the University of Nevada, Reno, NV, USA. He has coauthored 123 research publications and two patents. His research interests include plasma physics, high energy density physics, and fusion energy.

Prof. Bauer received the U.S. Presidential Early Career Award for Scientists and Engineers in 1997.

Glen A. Wurden (Senior Member, IEEE) was born in Anchorage, AK, in September 1955. He received three simultaneous B.S. degrees, in physics, mathematics, and chemistry (summa cum laude) from the University of Washington, Seattle, WA, USA, in 1977, and the M.S. and Ph.D. degrees in astrophysical sciences (plasma physics) from Princeton University, Princeton, NJ, USA, in 1979 and 1982, respectively.

He is currently a Senior Plasma Physicist with the Los Alamos National Laboratory, Los Alamos, NM, USA. His research interests include magnetized target fusion, plasma diagnostics, and alternate confinement concepts, including burning plasma issues.

Dr. Wurden is a fellow of the American Physical Society, the American Association for the Advancement of Science, and the Phi Beta Kappa.

Andrew S. Taylor, photograph and biography not available at the time of publication.

Derek A. Sutherland, photograph and biography not available at the time of publication.

Aaron Hossack received the B.S. degree in physics and astronomy and the Ph.D. degree in plasma physics from the University of Washington, Seattle, WA, USA, in 2009 and 2015, respectively.

He was a Research Associate and a Research Scientist at the Department of Aeronautics and Astronautics, University of Washington, from 2015 to 2023. Concurrently, he was the Co-Founder and the Chief Technology Officer with CTFusion, Inc., Seattle, from 2016 to 2023. He is currently a Research Scientist with Zap Energy, Inc., Everett, WA, USA. His research has been concerned with diagnostic techniques for and plasma physics of novel magnetic and magneto-inertial confinement of fusion plasmas.

Uri Shumlak (Fellow, IEEE) received the Ph.D. degree in nuclear engineering from the University of California at Berkeley, Berkeley, CA, USA, in 1992.

He was the National Research Council Post-Doctoral Fellow at the Air Force Phillips Laboratory, Albuquerque, NM, USA, where he authored MACH3, a 3-D, time-dependent magnetofluid code for nonideal plasmas in complex geometries. He is currently a Professor of aeronautics and astronautics with the Aerospace and Energetics Research Program, University of Washington, Seattle, WA, USA, where he is the Head of the ZaP Flow Z-Pinch Laboratory and the Computational Plasma Dynamics Group, which leads the development of the WARPX/WARPXM plasma simulation framework. He is also the Co-Founder and the Chief Scientist with Zap Energy-a spin-out company, University of Washington that is developing commercial nuclear fusion.

Prof. Shumlak is a fellow of the APS and an Associate Fellow of AIAA.

Ben J. Levitt, photograph and biography not available at the time of publication.

Brian A. Nelson, photograph and biography not available at the time of publication.

Morgan Quinley, photograph and biography not available at the time of publication.

Tobin R. Weber, photograph and biography not available at the time of publication.

Jared Smythe, photograph and biography not available at the time of publication.

Bennett Diamond, photograph and biography not available at the time of publication.

Marcus Parry, photograph and biography not available at the time of publication.

Clemente Parga, photograph and biography not available at the time of publication.